BOLETIN DE LA SOCIEDAD ESPAÑOLA DE
Cerámica y Vidrio
www.elsevier.es/bsecv

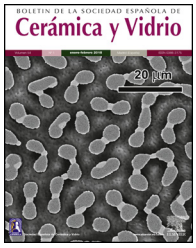

Drastic microstructural modification of $Bi_2Ca_2Co_2O_y$ ceramics by Na doping and laser texturing

Can Özçelik[b], *Tolga Depci*[b], *Mehmet Gürsul*[a], *Gizem Çetin*[a], *Bekir Özçelik*[a,*], *Miguel A. Torres*[c], *Maria A. Madre*[c], *Andres Sotelo*[c]

[a] *Department of Physics, Faculty of Sciences and Letters, Çukurova University, 01330 Adana, Turkey*
[b] *Iskenderun Technical University, Institute of Engineering and Sciences, Hatay, Turkey*
[c] *Institute of Nanoscience and Materials of Aragon (CSIC-Universidad de Zaragoza), Dpto. de Ciencia de Materiales, C/María de Luna 3, 50018 Zaragoza, Spain*

ARTICLE INFO

Article history:
Received 22 January 2021
Accepted 2 June 2021
Available online 20 June 2021

Keywords:
Ceramics
Oxides
Sintering
Texturing
Doping
Thermoelectrics

ABSTRACT

$Bi_2Ca_{2-x}Na_xCo_2O_y$ materials with $x = 0 \leq x \leq 0.125$, have been prepared either by sintering through the classical ceramic method, or textured using the laser floating zone technique. XRD results have shown that $Bi_2Ca_2Co_2O_y$ phase is the major one, independently of the Na content, in both kind of samples. SEM studies have shown a drastic microstructural modification between sintered and laser-textured materials. Na-doping increases density and grain sizes in sintered materials, while it enhances grain alignment in laser-grown materials. Moreover, it decreases secondary phase content in all cases. Electrical resistivity is also drastically reduced through texturing, when compared to the sintered samples, and Na-doping further decreases it. The lowest values determined in the laser-textured samples (26 mΩ cm at 650 °C) are around 40% lower than the best in sintered materials. On the other hand, S has been only slightly affected for Na-doping or processing method for all samples. Consequently, the highest power factor at 650 °C (0.18 mW/K^2 m) has been obtained in laser-grown 0.075Na-doped samples, which is around 20 and 70% higher than the measured in undoped laser-textured samples, and sintered ones, respectively.

Modificaciones drásticas en la microestructura de la cerámica $Bi_2Ca_2Co_2O_y$ inducidas por dopado con Na y texturado

Palabras clave:
Cerámicas
Óxidos

RESUMEN

Se han preparado materiales de composición $Bi_2Ca_{2-x}Na_xCo_2O_y$, con $x = 0 \leq x \leq 0{,}125$, por el método de estado sólido, además de texturarlos mediante la técnica de zona flotante inducida por láser. Los resultados de XRD han mostrado que la fase $Bi_2Ca_2Co_2O_y$ aparece como la mayoriraria, independientemente del contenido de Na, en ambos tipos de

* *Corresponding author.*
E-mail address: ozcelik@cu.edu.tr (B. Özçelik).
https://doi.org/10.1016/j.bsecv.2021.06.003

Sinterizado
Texturado
Dopado
Termoeléctricos

muestras. Los estudios SEM han encontrado una drástica modificación microestructural entre materiales sinterizados y texturados. El dopado con Na aumenta la densidad y el tamaño de grano en materiales sinterizados, mientras que mejora la orientación de los granos en materiales texturados. Además, disminuye el contenido de fases secundarias en todos los casos. La resistividad eléctrica disminuye drásticamente con el texturado, en comparación con las muestras sinterizadas, mientras que el dopado con Na la disminuye aún más. Los valores más bajos determinados en muestras texturadas (26 mΩ cm a 650 °C) son alrededor del 40% menor que los mejores datos publicados en materiales sinterizados. Por otro lado, S solo se ha visto afectado levemente, tanto por el dopado como por el método de procesado. En consecuencia, el máximo factor de potencia a 650 °C (0,18 mW/K^2 m) se ha obtenido en muestras dopadas con 0,075 Na y texturadas, que es alrededor de un 20 a un 70% superior al medido en muestras texturadas sin dopar y sinterizadas, respectivamente.

Introduction

Since the early years of thermoelectricity, many different families of materials with thermoelectric (TE) properties, have been discovered [1–3]. The main purpose of developing these materials is based on their ability to transform heat into electric power provided by the Seebeck effect [4]. The efficiency of this process is usually evaluated based on the materials properties using the dimensionless Figure-of-Merit (ZT) calculated through [5]:

$$ZT = \frac{S^2 T}{\rho k} \quad (1)$$

where S, ρ, κ, and T are Seebeck coefficient, electrical resistivity, thermal conductivity, and absolute temperature, respectively. In the above equation, the S^2/ρ relationship is called TE Power Factor (PF).

For practical purposes, it has been established that TE materials should have ZT $\geq$ 1 to be considered for applications. Until now, the materials presenting the highest ZT values are intermetallic materials, such as PbTeSe [1] or SnTe [6]. The main drawbacks of these materials are that they work properly at low-medium temperatures due to oxidation processes at high temperature under air, and their high costs [4], and low abundance in the earth crust [7]. Other promising materials are silicides [8] but, in spite of the large abundance of silicon in the earth crust [7], the best performances are obtained in compounds including high costs elements [4]. On the other hand, oxide materials with relatively high TE performances were discovered in 1997 [3]. These materials combine high thermal stability and working temperatures, low costs, and relatively high abundance in the earth crust [4,7]. This discovery, and these advantages of oxide materials, led to new families with attractive TE properties, such as $Bi_2AE_2Co_2O_x$ (AE: alkaline earth) [9,10]. The main concern about these materials was their typically low TE performances, showing ZT values below 1, but the interest about them was increased when ZT values of 1.2 in $Bi_2Sr_2Co_{1.8}O_x$ whiskers were reported [11]. However, despite the many works performed on TE oxides, bulk polycrystalline materials have not yet reached these ZT values. Consequently, one of the most important objectives is the enhancement of their TE performances before they can be used in practical applications. Among the different strategies for enhancing TE properties of these oxide materials, some like using soft chemistry methods [12,13], texturing [14,15], or doping [16,17] can be highlighted.

Other studies about the crystallographic structure of these CoO-based materials have shown that they can be described using a monoclinic structure, which is formed by two alternatively stacked layers. These layers can be, in turn, described as a conductive CdI_2-type hexagonal CoO_2 layer, and a rock-salt-type (RS) one. Both sublattices possess common a- and c-axis lattice parameters and β angles but different b-axis length, causing a misfit along the b-direction [18]. As a consequence of this structure, it has been found that cationic substitution in the RS layer using a lower oxidation cation, increases the charge carrier concentration in the conduction band due to the partial promotion of Co^{3+} cations to Co^{4+} in the conducting layer [19]. On the other hand, as the thermoelectric parameters are linked each other, a decrease of Seebeck coefficient, is also produced [20]. This effect can be produced in CoO-based materials by partially substituting an alkaline earth with an alkaline element, as previously reported [21,22].

The objective of this work is evaluating the modifications in structural, microstructural, and thermoelectric properties of $Bi_2Ca_2Co_2O_x$ materials through partial substitution of Ca^{2+} by Na^+. These modifications will be evaluated in laser-textured materials using as reference classically sintered samples with the same composition.

Experimental

$Bi_2Ca_{2-x}Na_xCo_2O_y$ precursors, with x ranging between 0 and 0.125, were obtained from commercial Bi_2O_3 (98+%, Panreac), $CaCO_3$ (98.5%, Panreac), CoO (99.99%, Sigma–Aldrich), and Na_2CO_3 (99.8%, Panreac) starting powders. They have been weighed in the respective stoichiometric proportions, and ball milled in an agate ball-mill, using water media, at 300 rpm for 30 min. These suspensions were then totally dried under IR radiation, and calcined using a two-steps process, at 750 °C for 12 h, and 800 °C for another 12 h, with an intermediate manual milling, to produce a fine powder. Following this thermal procedure, Ca and Na carbonates are mostly decomposed and the

different oxides start to react, as previously reported [23]. Part of these powders has been cold uniaxially pressed into pellets under 400 MPa applied pressure, and sintered at 810 °C for 24 h with a final furnace cooling. The other part of precursors has been cold isostatically pressed in form of cylinders (~3 mm diameter) under 200 MPa, and used as feed in a laser floating zone (LFZ) device described elsewhere [24]. The molten zone has been induced by a Nd:YAG laser radiation (Spectron Laser Systems, $\lambda = 1024$ nm), and the growth conditions were fixed at 30 mm/h. Moreover, the seed has been rotated at 3 rpm to keep the cylindrical geometry while the feed has been oppositely rotated at 15 rpm to maintain the compositional homogeneity in the molten zone. After this process, cylindrical laser-textured materials (~2 mm diameter), have been obtained. However, these Bi-containing compounds typically show incongruent melting, leading to a complex mixture of secondary phases in the bulk material after solidification [10,14]. Consequently, following texturing process, it is necessary to perform an annealing procedure at 800 °C for 24 h to obtain the thermoelectric phase from the secondary ones [14].

Powder X-ray diffraction (XRD) data of all prepared samples were recorded at room temperature in a Rigaku D/max-B X-ray powder diffractometer (Cu Kα radiation), with 2θ ranging between 10° and 40°, in order to identify the phases in the sintered and laser-textured materials. SEM characterization has been performed in a Zeiss-Merlin field emission scanning electron microscope (FESEM), associated to an energy-dispersive spectroscopy (EDS) system used for qualitative elemental analysis. Samples were analysed, using backscattered electrons, on longitudinal polished sections to determine the microstructural and compositional modifications induced by Na doping and texturing process.

Electrical resistivity and Seebeck coefficient were simultaneously determined between room temperature and 650 °C, under He atmosphere. For this purpose, the standard dc four-probe configuration, in steady-state conditions, has been used in a LSR-3 system (Linseis GmbH). The measurements have been performed on heating, with a dwell time of 30 s before each measurement, and setting a fixed temperature gradient of 30 °C between the ends of the samples. The samples were measured along the growth axis, which coincides with the conducting plane of $Bi_2Ca_2Co_2O_y$ phase. Finally, from these electrical resistivity and Seebeck coefficient data, the thermoelectric performances of samples, evaluated through their PF, have been calculated to stablish the influence of Na-doping and texturing on the thermoelectric characteristics of these materials. Moreover, these values will be also compared to the best results presented in literature.

Results and discussion

Representative XRD patterns obtained on grinded $Bi_2Ca_{2-x}Na_xCo_2O_y$ samples are shown in Fig. 1. In this plot, it can be observed that most of the peaks (indicated by their diffraction planes) can be associated to the thermoelectric $Bi_2Ca_2Co_2O_y$ phase, as the major one independently of the processing technique, in agreement with previously reported data [23]. Moreover, the * shows the Co-free $Ca_4Bi_6O_{13}$ secondary phase [25], which should be in small proportions due to the low intensity of its diffraction peaks. From these data, it can be easily deduced that all samples are formed by nearly single $Bi_2Ca_2Co_2O_y$ phase. On the other hand, it can be seen that undoped samples show slightly higher amount of Co-free secondary phase than doped ones, and that laser-grown samples also possess lower amount than sintered ones. Consequently, it can be established that laser-texturing decreases the secondary phase content, which is further decreased by Na doping. Furthermore, detailed observation of the different patterns has shown that no shift is produced in the thermoelectric phase diffraction peaks, independently of the Na content, or the processing route. Besides Lotgering factor (LF) is a useful parameter to quantify variation of grain orientation which defines as $LF = (P - P_0)/(1 - P_0)$, where P indicates the fraction of the summation of the peak intensities of preferred orientation and P_0 is the P of the samples with a non-oriented distribution [26]. The calculated values for sintered and laser-textured samples are displayed in Table 1. From these results, it can be easily observed that LFZ process, together with Na-substitution clearly raises grain orientation, when compared to the sintered materials.

Fig. 2 presents SEM micrographs performed on the longitudinal polished surface of representative $Bi_2Ca_{2-x}Na_xCo_2O_y$ samples. In these micrographs, three different contrasts can be observed (identified in the pictures for clarity). These contrasts have been associated through EDS to different phases: #1 (grey) corresponds to the thermoelectric phase, while #2, and #3 (light and dark grey) have been identified as Bi-Ca oxide, and Co oxide, respectively. Moreover, the drastic microstructure modifications between sintered (Fig. 2a, and c) and laser-grown (Fig. 2b, and d) samples can also be seen. Sintered samples display randomly oriented grains, and a small amount of Co oxide in the undoped samples. When Na is added, it induces a decrease of porosity, and the amount of Co oxide, while increasing grain sizes. On the other hand, laser-textured samples present longer grains, aligned along the growth direction, with much lower amount of porosity and Co oxide phase, when compared to the sintered ones. Furthermore, Na addition slightly increases grain alignment and decreases the amount of both secondary phases. The microstructural modifications produced by Na doping in the sintered and laser-grown samples can be associated to the formation of a Bi_2O_3-Na_2CO_3 eutectic, as it has been found that melting point of Na-doped samples is slightly decreased when compared to the undoped ones, in agreement with previous works in similar systems [21]. The presence of this eutectic can explain the large grain growth produced in Na-doped samples when compared to the undoped ones (see Fig. 2a, and c), due to the enhancement of cation mobility, and the better alignment observed in Na-doped laser-textured samples (see Fig. 2b, and d).

Electrical resistivity evolution with temperature, as a function of Na content, for both types of samples, is displayed in Fig. 3. In the graph, it can be easily observed that the sintered samples (Fig. 3a) possess higher electrical resistivity than laser-textured ones (Fig. 3b), in the whole measured temperature range. This behaviour clearly reflects the different microstructure previously discussed, as long and well oriented grains, together with much lower porosity, lead to decreased resistivity values in the laser-grown materials. Moreover, the

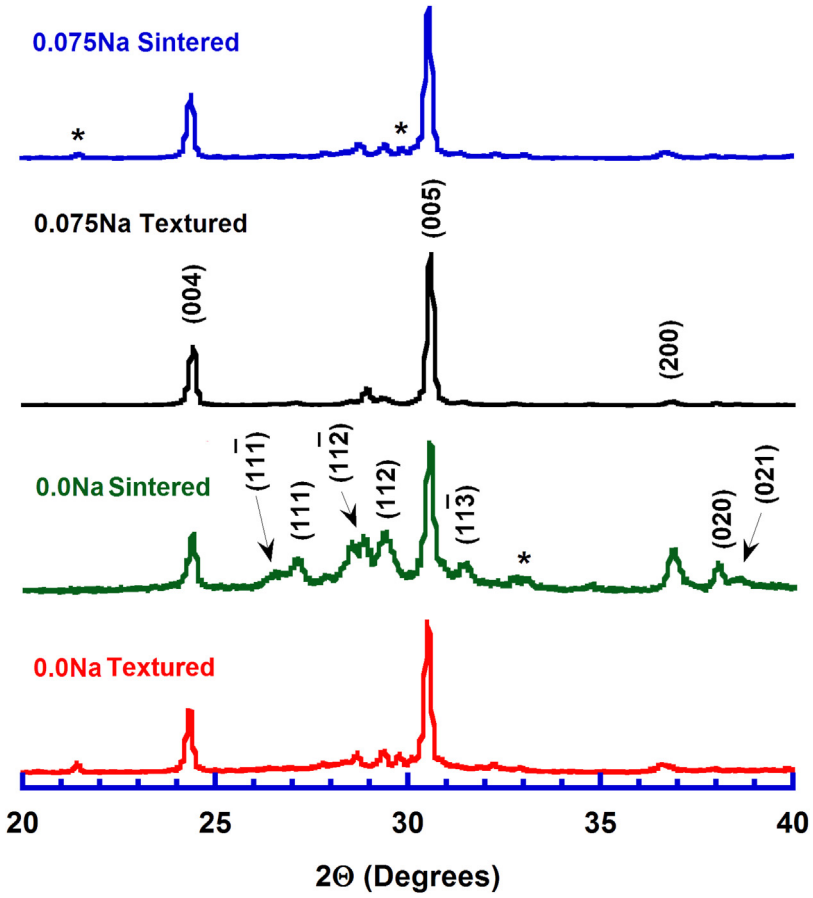

Fig. 1 – Representative powder X-ray diffraction patterns of different $Bi_2Ca_{2-x}Na_xCo_2O_y$ samples. Diffraction planes show the peaks of the TE phase, while * identifies the one of the Bi-Ca—O (Co-free) phase.

Table 1 – Lotgering factor determined in the different samples.

Na substitution-level	Sintered LF	Textured
0	0.41	0.78
0.05	0.70	0.80
0.075	0.72	0.82
0.10	0.75	0.84
0.125	0.80	0.82

minimum resistivity values have been obtained in 0.10Na-doped samples in both cases, evidencing the favourable effect of grain orientation on the electrical conduction. The main difference between both types of samples, besides the magnitude of the electrical resistivity, is its evolution with temperature. In this regard, undoped sintered samples show semiconducting behaviour ($d\rho/dT<0$) from room temperature to around 400 °C, being metallic one ($d\rho/dT>0$) at higher temperatures (see Fig. 3a). When Na is added to these samples, the transition temperature between semiconducting and metallic behaviour is decreased to about 300 °C for 0.05Na-doped samples, and lower resistivity variations. Further Na-doping leads to metallic behaviour in the whole measured temperature range. Furthermore, as previously mentioned, electrical resistivity is decreased when the amount of Na is increased up to 0.10, increasing for further Na addition. This evolution is in agreement with the fact that substituting Ca^{2+} with Na^{+} lead to reduces the total charge in the RS layer which, in turn, increases the oxidation state of Co^{3+} to Co^{4+} in the conducting layer. This process increases the charge carrier concentration in the conduction band, reducing electrical resistivity. However, the slightly different ionic size of Ca^{2+} and Na^{+} lead to a decrease of charge carrier mobility, tending to increase electrical resistivity. Consequently, the observed behaviour of these samples can be explained by a combination of these two previously discussed effects, increasing or decreasing resistivity as a function of the predominant one.

When considering the evolution of laser-textured samples (Fig. 3b), undoped and 0.05Na-doped ones present semiconducting behaviour in the whole measured temperature range, 0.075 and 0.125Na-doped change to metallic at around 400 °C, and 0.10Na samples are metallic at all temperatures. This evolution can be explained taking into account the same discussion made for the sintered samples, but adding new parameters: the drastic grain alignment, and the LFZ technique, which produces a high number of oxygen vacancies in the thermoelectric phase, usually not totally filled after the annealing procedure. As a consequence of these vacancies, Co^{4+} in the conduction layer is reduced to Co^{3+}, as previously observed in related systems [26,27], tending to

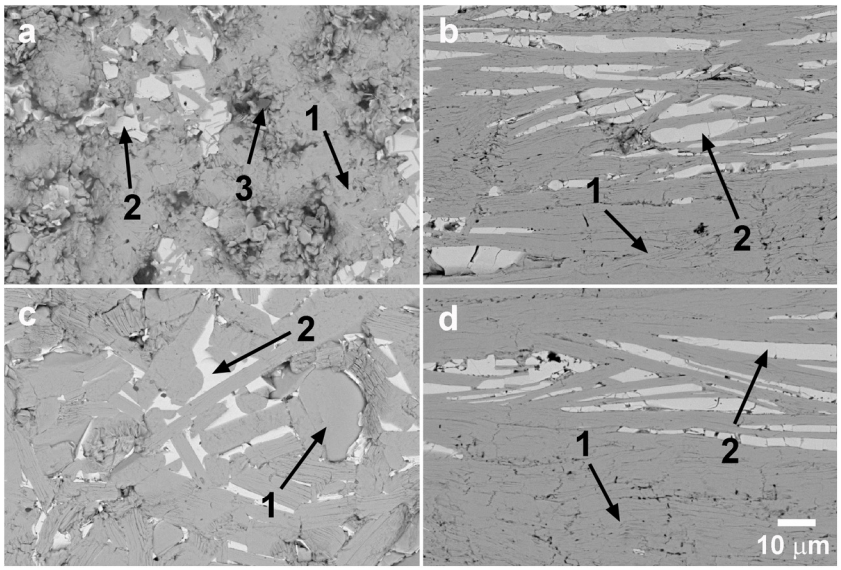

Fig. 2 – Representative SEM micrographs performed longitudinal polished surfaces of (a and c) sintered; and (b and d) textured samples, with composition $Bi_2Ca_2Co_2O_y$ (a, and b); and $Bi_2Ca_{1.925}Na_{0.075}Co_2O_y$ (c, and d). Grey contrast (#1) corresponds to the thermoelectric phase, light grey (#2) to the Co-free one (Bi—Sr—O), and black one (#3) to Co-oxide.

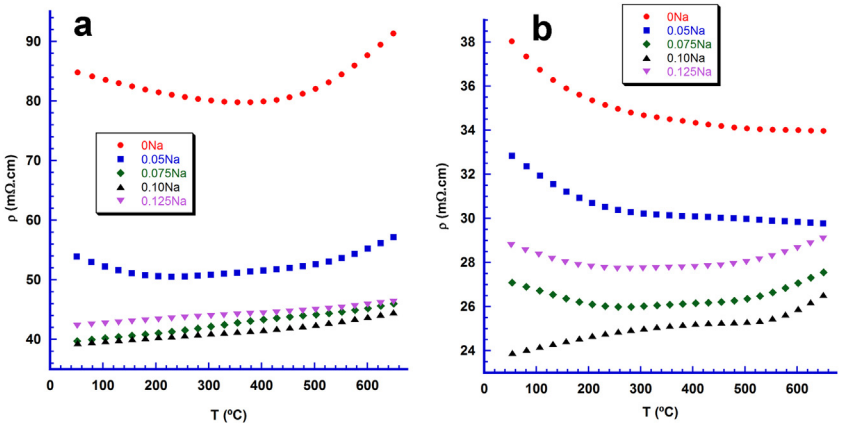

Fig. 3 – Electrical resistivity evolution with temperature in $Bi_2Ca_{2-x}Na_xCo_2O_y$ samples (a) sintered; and (b) textured.

increase electrical resistivity. The lowest resistivity values at 650 °C (26 mΩ cm) have been determined in 0.10Na substituted laser-textured samples, which is about 40% lower than those obtained in undoped laser-textured samples, and around 80% lower than the lowest value obtained in sintered samples in this work. Moreover, these values are much lower than the best reported sintered materials prepared through solution methods (50 mΩ cm) [28], and in the order of textured materials using hot uniaxial pressing process (28 mΩ cm) [29]. These results clearly agree with the large grain sizes and orientation, and the decrease of porosity in LFZ grown samples.

Fig. 4 displays Seebeck coefficient variation with temperature, and Na substitution for both kind of samples. In the graph, it can be seen that all samples present positive values in the whole measured temperature range, characteristic of hole-dominating transport mechanism. Moreover, S increases with temperature in all cases, which is the typical behaviour of a degenerate semiconductor, in agreement with previous works [26,28,29]. In general, laser-grown materials show higher S values at room temperature than the sintered ones, in agreement with the previous discussion showing that LFZ processing induces a large number of oxygen vacancies which are not totally filled by annealing. Consequently, the amount of Co^{3+} in the conduction layer is increased, leading to higher S values, in agreement with Koshibae's expression [20]. On the other hand, at high temperatures the S values are very similar for both kind of samples, being slightly higher for the samples which displayed higher electrical resistivity values, due to their lower Na content. The highest values (220 μV/K) have been measured in undoped sintered, as well as in undoped and 0.05Na-doped textured, materials. These values are very similar to the obtained in sintered materials produced using solution methods (218 μV/K) [28], or hot uniaxially pressed (230 μV/K) [29]. On the other hand, they are much lower than

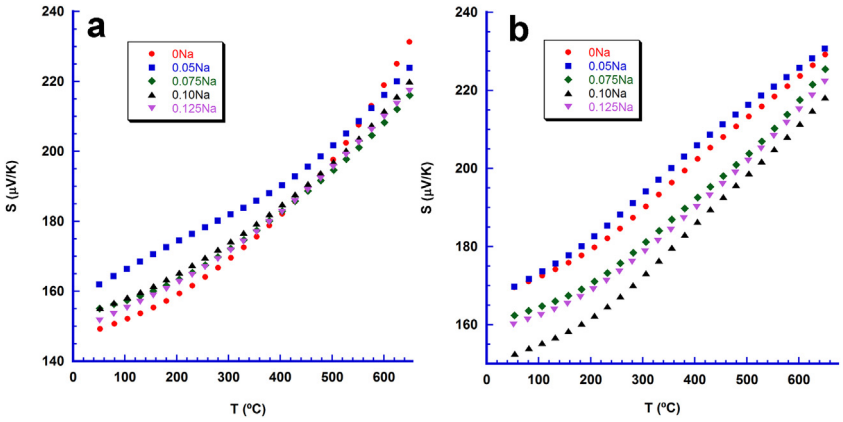

Fig. 4 – Seebeck coefficient evolution with temperature in $Bi_2Ca_{2-x}Na_xCo_2O_y$ samples (a) sintered; and (b) textured.

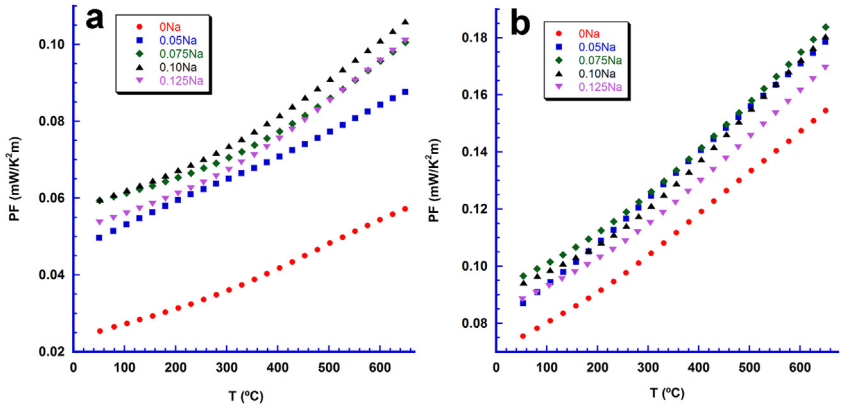

Fig. 5 – Power Factor evolution with temperature in $Bi_2Ca_{2-x}Na_xCo_2O_y$ samples (a) sintered; and (b) textured.

the determined in LFZ as-textured materials (268 μV/K) [23] due to their high content of oxygen vacancies.

PF evolution with temperature, obtained from the electrical resistivity and Seebeck coefficient data, is presented in Fig. 5 for both types of samples. As it can be observed in the graphs, laser-textured samples show much higher PF values than the sintered ones, due to their lower electrical resistivity and similar S values. These results clearly show the beneficial effect of grain alignment and density over the amount of secondary phases, in the thermoelectric performances of these materials. In spite of these different values, the behaviour of all samples is very similar; PF grows with temperature in the whole measured temperature range, and the highest values in each type of samples are reached in medium Na content ones: 0.10 sintered, and 0.05, 0.075, and 0.10Na laser-textured samples. The highest value determined in laser-grown samples (0.18 mW/K^2 m) is around 20 and 70% higher than the measured in undoped laser-textured samples, and sintered ones, respectively. Moreover, it is much higher than the reported for as-grown materials (0.085 mW/K^2 m) [23], and sintered materials produced through solution methods (0.09 mW/K^2 m) [28]. On the other hand, it is lower than the measured in hot uniaxially pressed materials treated for 50 h (0.25 mW/K^2 m) [29]. Despite of this slightly lower performances, the process to obtain the samples in this work is very simple and allows obtaining the samples with adequate geometry to be directly integrated in thermoelectric modules without further machining.

Conclusions

$Bi_2Ca_{2-x}Na_xCo_2O_y$ ($0 \leq x \leq 0.125$) thermoelectric ceramics have been successfully prepared through the classical ceramic route, and textured through the LFZ method. It has been found that Na substitution leads to a drastic grain growth in the sintered materials, and a slight improvement of grain orientation in the laser-textured ones. Moreover, it decreases secondary phases in both kind of samples. The microstructural differences between sintered and laser-grown materials have been reflected in a drastic decrease of electrical resistivity, with no significant reduction of Seebeck coefficient. On the other hand, Na-doping decreases electrical resistivity up to 0.10 in both types of samples. The increase of electrical resistivity in samples with higher Na content is associated to the raise of defects which act as electronic scattering centers. All these characteristics led to much higher power factor values in laser-textured samples, when compared to the sintered ones. Further increase is produced, in both cases, in Na substituted samples. These improvements, and the possibility to use these

samples directly in thermoelectric modules, make them very interesting ceramic materials for practical applications.

Acknowledgements

This study was carried out within the scope of Cukurova University Scientific Research Projects Unit FBA-2020-13007. The authors wish to thank the Spanish MINECO-FEDER (MAT2017-82183-C3-1-R), and Gobierno de Aragón (Research Group T 54-20 R) for funding. The authors wish to acknowledge the use of Servicio General de Apoyo a la Investigación-SAI, Universidad de Zaragoza.

REFERENCES

[1] T. Fu, X. Yue, H. Wu, C. Fu, T. Zhu, X. Liu, L. Hu, P. Ying, J. He, X. Zhao, Enhanced thermoelectric performance of PbTe bulk materials with figure of merit zT > 2 by multi-functional alloying, J. Materiomics 2 (2016) 141–149.

[2] E.N. Nikitin, Study of temperature dependencies of electrical conductivity and thermal power of silicides, Zhurnal Tekhnicheskoj Fiziki 28 (1958) 23–25.

[3] I. Terasaki, Y. Sasago, K. Uchinokura, Large thermoelectric power in $NaCo_2O_4$ single crystals, Phys. Rev. B 56 (1997) 12685–12687.

[4] S. LeBlanc, Thermoelectric generators: linking material properties and systems engineering for waste heat recovery applications, Sust. Mater. Technol. 1–2 (2014) 26–35.

[5] D.M. Rowe. In: D.M. Rowe, editor. Thermoelectrics Handbook: Macro to Nano. 1st ed. Boca Raton, FL: CRC Press; 2006.

[6] H.C. Wang, J. Hwang, C. Zhang, T. Wang, W.B. Su, H. Kim, J. Kim, J.Z. Zhai, X. Wang, H. Park, W.C.L. Wang, Enhancement of the thermoelectric performance of bulk SnTe alloys via the synergistic effect of band structure modification and chemical bond softening, J. Mater. Chem. A 5 (2017) 14165–14173.

[7] J. He, Y. Liu, R. Funahashi, Oxide thermoelectrics: the challenges, progress, and outlook, J. Mater. Res. 26 (2011) 1762–1772.

[8] D.C. Ramirez, L.R. Macario, X.Y. Cheng, M. Cino, D. Walsh, Y.C. Tseng, H. Kleinke, Large scale solid state synthetic technique for high performance thermoelectric materials: magnesium-silicide-stannide, ACS Appl. Energy Mater. 3 (2020) 2130–2136.

[9] R. Funahashi, I. Matsubara, S. Sodeoka, Thermoelectric properties of $Bi_2Sr_2Co_2O_x$ polycrystalline materials, Appl. Phys. Lett. 76 (2000) 2385–2387.

[10] M.A. Madre, F.M. Costa, N.M. Ferreira, S.I.R. Costa, Sh. Rasekh, M.A. Torres, J.C. Diez, V.S. Amaral, J.S. Amaral, A. Sotelo, High thermoelectric performance in $Bi_{2-x}Pb_xBa_2Co_2O_x$ promoted by directional growth and annealing, J. Eur. Ceram. Soc. 36 (2016) 67–74.

[11] R. Funahashi, M. Shikano, $Bi_2Sr_2Co_2O_y$ whiskers with high thermoelectric figure of merit, Appl. Phys. Lett. 81 (2002) 1459.

[12] A. Sotelo, Sh. Rasekh, M.A. Torres, P. Bosque, M.A. Madre, J.C. Diez, Effect of synthesis methods on the $Ca_3Co_4O_9$ thermoelectric ceramic performances, J. Solid State Chem. 221 (2015) 247–254.

[13] N.Y. Wu, T.C. Holgate, N.V. Nong, N. Pryds, S. Linderoth, High temperature thermoelectric properties of $Ca_3Co_4O_{9+\delta}$ by auto-combustion synthesis and spark plasma sintering, J. Eur. Ceram. Soc. 34 (2014) 925–931.

[14] Sh. Rasekh, F.M. Costa, N.M. Ferreira, M.A. Torres, M.A. Madre, J.C. Diez, A. Sotelo, Use of laser technology to produce high thermoelectric performances in $Bi_2Sr_2Co_{1.8}O_x$, Mater. Des. 75 (2015) 143–148.

[15] H. Wang, X. Sun, X. Yan, D. Huo, X. Li, J.-G. Li, X. Ding, Fabrication and thermoelectric properties of highly textured $Ca_9Co_{12}O_{28}$ ceramic, J. Alloys Compd. 582 (2014) 294–298.

[16] N. Sun, S.T. Dong, B.B. Zhang, Y.B. Chen, J. Zhou, S.T. Zhang, Z.B. Gu, S.H. Yao, Y.F. Chen, Intrinsically modified thermoelectric performance of alkaline-earth isovalently substituted $[Bi_2AE_2O_4][CoO_2]_y$ single crystals, J. Appl. Phys. 114 (2013) 043705.

[17] A.I. Klyndyuk, I.V. Matsukevich, Synthesis, structure, and properties of $Ca_3Co_{3.85}M_{0.15}O_{9+\delta}$ (M = Ti–Zn, Mo, W Pb, Bi) layered thermoelectrics, Inorg. Mater. 51 (2015) 944–950.

[18] A. Maignan, S. Hebert, M. Hervieu, C. Michel, D. Pelloquin, D. Khomskii, Magnetoresistance and magnetothermopower properties of Bi/Ca/Co/O and Bi(Pb)/Ca/Co/O misfit layer cobaltites, J. Phys.: Condens. Matter 15 (2003) 2711–2723.

[19] A. Maignan, D. Pelloquin, S. Hebert, Y. Klein, M. Hervieu, Thermoelectric power in misfit cobaltites ceramics: optimization by chemical substitutions, Bol. Soc. Esp. Ceram. V 45 (2006) 122–125.

[20] W. Koshibae, K. Tsutsui, S. Maekawa, Thermopower in cobalt oxides, Phys. Rev. B 62 (2000) 6869–6872.

[21] G. Çetin Karakaya, B. Ozcelik, O. Nane, A. Sotelo, Sh. Rasekh, M.A. Torres, M.A. Madre, Improvement of $Bi_2Sr_2Co_2O_y$ thermoelectric performances by Na doping, J. Electroceram. 40 (2018) 11–15.

[22] Y.-N. Li, P. Wu, S.-P. Zhang, S. Chen, D. Yan, J.-G. Yang, L. Wang, X.-L. Huai, Thermoelectric properties of lower concentration K-doped $Ca_3Co_4O_9$ ceramics, Chin. Phys. B 27 (2018) 057201.

[23] Sh. Rasekh, M.A. Madre, A. Sotelo, E. Guilmeau, S. Marinel, J.C. Diez, Effect of synthetic methods on the thermoelectrical properties of textured $Bi_2Ca_2Co_{1.7}O_x$ ceramics, Bol. Soc. Esp. Ceram. V 49 (2010) 89–94.

[24] F.M. Costa, N.M. Ferreira, Sh. Rasekh, A.J.S. Fernandes, M.A. Torres, M.A. Madre, J.C. Diez, A. Sotelo, Very large superconducting currents induced by growth tailoring, Cryst. Growth Des. 15 (2015) 2094–2101.

[25] J.B. Parise, C.C. Torardi, M. Whangbo, C.J. Rawn, R.S. Roth, B.P. Burton, $Ca_4Bi_6O_{13}$, a compound containing an unusually low bismuth coordination number and short Bi–Bi contacts, Chem. Mater. 2 (1990) 454–458.

[26] A. Sotelo, E. Guilmeau, M.A. Madre, S. Marinel, S. Lemonnier, J.C. Diez, $Bi_2Ca_2Co_{1.7}O_x$ thermoelectric ceramics textured by laser floating zone method, Bol. Soc. Esp. Ceram. V 47 (2008) 225–228.

[27] M. Karppinen, H. Fjellvag, T. Konno, Y. Morita, T. Motohashi, H. Yamauchi, Evidence for oxygen vacancies in misfit-layered calcium cobalt oxide, $[CoCa_2O_3]_{(q)}CoO_2$, Chem. Mater. 16 (2004) 2790–2793.

[28] A. Sotelo, Sh. Rasekh, M.A. Madre, E. Guilmeau, S. Marinel, J.C. Diez, Solution-based synthesis routes to thermoelectric $Bi_2Ca_2Co_{1.7}O_x$, J. Eur. Ceram. Soc. 31 (2011) 1763–1769.

[29] E. Guilmeau, M. Mikami, R. Funahashi, D. Chateigner, Synthesis and thermoelectric properties of $Bi_{2.5}Ca_{2.5}Co_2O_x$ layered cobaltites, J. Mater. Res. 20 (2005) 1002–1008.